RSC Advances

ROYAL SOCIETY OF CHEMISTRY

www.rsc.org/advances

Journal Name

RSCPublishing

ARTICLE

3D controllable preparation of composite CuO/TiO_2 nanofibers

Cite this: DOI: 10.1039/xoxxoooooox

Fanli Zhang[a], Zhiqiang Cheng*[a,b], Lijuan Kang[a], LiYing Cui[a], Wei Liu[a], Guohui Hou[a], Hongjia Yang[a], Xiaojuan Xu[a]

Received ooth January 2014,
Accepted ooth January 2014

DOI: 10.1039/xoxxoooooox

www.rsc.org/

The preparation and research of nanometer metal oxide has been drawn much attention for the special structure and excellent chemical properties especially titania and titanium dioxide composite nanomaterials. A three-dimensional (3D) multiple-unit semiconductor CuO/TiO_2 film was successfully synthesized by the combination of electrospinning and hydrothermal reaction. The samples were characterized by Differential Thermal Analyzer (TG-DTA) X-ray Diffraction (XRD), Transmission Electron Microscopy (TEM), Scanning Electron Microscope (SEM) which indicated the diameter of the TiO_2 fibers were about < 100 nm; the CuO nanoparticles or nanoplates were growing aslant on the surface of TiO_2 fibers, which led to the porous morphology for the hierarchical heterostructure. The photocatalytic property of the samples was tested via rhodamine B degradation and it showed the obvious catalytic activity for the Simulation of pollutants. Furthermore, the photocatalytic mechanism about the CuO/TiO_2 nanofiber was expounded at the end of paper.

Introduction

It was in 1972 since the scientist of Japan fujishima discovered the performance of TiO_2 in photocatalytic hydrogen production,[1] it has attracted lots of attention of scientific researchers in the world widely; so the TiO_2 has been applied in a variety of fields from now on, such as photocatalytic degradation,[2] the solar cell,[3] gas sensor,[4] biosensor[5] and other fields in industrial catalysis. As a result of TiO_2 in the photocatalytic degradation of organic pollutants[6] in the process of high activity, non-toxic, chemically stability, refractory, long-term light corrosion and chemical corrosion resistance,[7-9] it shows bright prospect in photocatalytic aspects. Although the good prospect of application in photocatalysis, there are also some defects in the quantum efficiency[10], Sunlight utilization,[11,12] recycling and photon-generated carrier problems. At the same time, the TiO_2 structure, size and composition will play the great role in its photocatalytic performance.[13-19] So in order to make full use of green pollution-free solar energy and improve the photocatalytic activity of TiO_2, it usually need some decorations, such as the surface of the precious metal deposition, ion doping, dye sensitizing, coupled semiconductor. Coupled Semiconductor is a kind of effective method to improve the property of TiO_2 in photocatalysis.[20] It is universally acknowledged that the CuO in the nanoscale will appear great catalytic activity[21] for the low band gap. Because of the nanostructure and physical property of CuO, it is also widely used as gas sensor[22,23] and antibacterial materials.[24]

[a]*Institute of resources and environment, Jilin agricultural university, ChangChun of JiLin province 130000, People's Republic of China*

[b]*Institute of aeronautics and astronautics, Tsinghua university, BeiJing, 100000, China. E-mail: czq5974@163.com*

Based on the motheds of predecessor,[25] we have firstly synthesized the 3-D composite nanometer CuO/TiO_2 hierarchical heterostructure which is nanoporous on the surface of the fibers and easy to be recycled with combination of electrospinning technique and hydrothermal synthesis method. Before the thesis writing, we have done a lot of work in controlling the morphology of the CuO doping on the TiO_2 fibers surface by adjusting the reaction temperature, alkali source, cupper ion concentration and other experiment parameters. The main factors which affect the morphology of the CuO/TiO_2 films were alkali source and the reaction temperature. In the process of photocatalytic degradation for rhodamine B (RhB) which is typical model organic pollutants, the as-prepared showed an obvious degradation effect for it. So it is beneficial exploration for the S-S type semiconductor compounds.

Experimental section

Materials and methods

First, the TiO_2 sol was prepared by 5.00 g of tetrabutyl titanate ($Ti(OBu)_4$ 97 %, Sigma-Aldrich) with a mixture of 23mL of methyl alcohol (99.5 % Beijing chemical works) and 0.3 mL of acetic acid (99.5 % Beijing chemical works). Next, 1.40 g Polyvinylpyrrolidone (PVP Mw~1 300 000, Sigma-Aldrich) was added to the TiO_2 sol solution. The precursor mixture was stirred for 12 hours at room temperature to attain Uniform, transparent, light green solution required for electrospinning and then the solution was loaded into a syringe. The feeding rate of the solution in the syringe was controlled at 1.0 mL h^{-1}. The voltage applied to the needle of the syringe was 12 kV and the distance from the tip of the needle and the aluminum foil collector was 13~15 cm at a fume hood in air with the

humidity of below the 40 %. After the obtained non-woven film was calcined at 520 ℃ in 4 hours. Then the electro-spinning TiO_2 fibrous film was put into an autoclave containing $Cu(Ac)_2 – C_6H_{12}N_4 – H_2O$ (CT1 sample), $Cu(Ac)_2 – NH_3•H_2O – H_2O$ (CT2 sample) solution respectively and the concentrations of Cu^{2+}, $C_6H_{12}N_4$ and $NH_3•H_2O$ were 0.1 M, 1.2 M and 13.33 M (Room temperature about 25 w_t %). The hydrothermal reaction was carried out at 120 ℃ for 10 hours. The as-prepared products would be easily collected and then washed with deionized water and ethanol absolute at last.

Characterization

The X-ray diffraction (XRD) patterns of the samples were measured on D/MAX 2250 V diffractometer (Rigaku Japan), using Cu Kα (λ=0.15418 nm) radiation under 40 kV, 30 mA and scanning over the range of 20°~80°. The morphologies and microstructures of as-prepared samples were characterized by the Scanning Electron Microscope (SEM, SHIMADZU X-550) and High Resolution Transmission Electron Microscopy (HRTEM, Tecnai G2). UV-vis absorption spectra were recorded on an UV-vis spectrophotometer (Hitachi U-3010). The as-spun PVP/TiO_2 composite nanofibers were subjected to Thermogravimetric Differential Thermal Analysis (TG–DTA, HCT-3).

Photocatalytic experiments

Photocatalytic performance of the as-prepared samples was evaluated by the degradation of rhodamine B. The photo-catalytic degradation of RhB in the liquid phase was conducted in an ordinary glass of 250 ml with the condensing equipment at the room tempreture. The glass reactor was illuminated by the wideband lamp bulb (25 W Philips TL/05) with a predominant wavelength of 365 nm; The vertical distance between the glass reactor and the lamp was 15cm; Then 100 ml (10 mg L^{-1}) RhB solution was mixed with 0.10 g sample; prior to irradiation, the mixed solution was magnetically stirred in the dark for 30 minutes to ensure the establishment of an adsorption/desorption equilibrium between the CuO/TiO_2 films and the RhB dye. An aliquot (3 mL) of the solution was taken at half an hour interval during the experiment and tested on the Varian UV-vis spectrophotometer (Hitachi U-3010). As a comparison, an RhB photolysis process without CuO/TiO_2 films was also performed under the same conditions. After every assay, the analyzed aliquot was poured back into the glass reactor immediately to ensure a roughly equivalent volume of solution. Each catalytic experiment lasted for three hours in all. The change of RhB absorbance was used to monitor the extent of reaction at given irradiation time intervals.

Results and discussion

Characterization of CuO/TiO_2 nanofibers

The results of simultaneous TG and DTA analyses of the as-spun TiO_2/PVP composite nanofibers are shown in Fig.1. The whole process is divided into three regions. The range of 30 ℃~150 ℃ is the first part and there is an unconspicuous endothermic peak at 75 ℃ in DTA curve, which indicates the loss of moisture about 10 % from the composite fibers surface and residual moisture in internal fibers. The second part is 275 ℃ to 400 ℃ from DTA curve and there are two apparent exothermic peaks at 315 ℃ and 390 ℃, which represent the decomposition of branched chain of PVP and the process of the formation for anatase phase respectively.[26] In this section, Weightlessness rate is about 30.4 %. From 400 ℃ to 520 ℃ is the last part, the weight loss ratio about 20.4 %, which is mainly for the degradation of main chain of PVP until 520 ℃. Therefore, the obtained non-woven film was calcined to form TiO_2 fibrous film at 520 ℃.

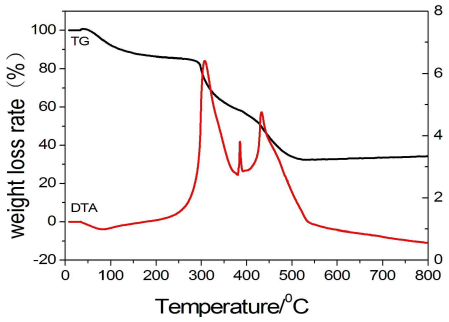

Fig.1 Thermal gravimetry– differential thermal analysis (TG-DTA) curves of PVP/TiO_2

The hierarchical heterostructure of the CuO/TiO_2 sample was shown in Figure.2C; the SEM image Fig.2A shows that the TiO_2 fiber surface was smooth, which indicates that TiO_2 was uniformly dispersed in the PVP/TiO_2 mixture. The statistical tables on the Fig.2A and Fig.2C respectively for diameter of the statistics of TiO_2 fibers and CT1 of CuO/TiO_2 fibers showed that the diameter of TiO_2 fibers increased due to the adjunction of the nanostructural CuO after the hydrothermal treatment. Therefore, we observed the SEM Fig.2A and Fig.2C images and tested the diameter of 100 fibers before and after hydrothermal treatment respectively. The statistical graph revealed that the distribution of TiO_2 fibers diameter mainly ranged from 20~110nm amount to 72 %, 93 nm in average and there were 80 % of the CuO /TiO_2 fibers which were 300~450 nm, 381 nm in average. The CuO layer thickness was about 125 nm to 165 nm and we could control the thickness of CuO by adjusting the concentration of copper ions.

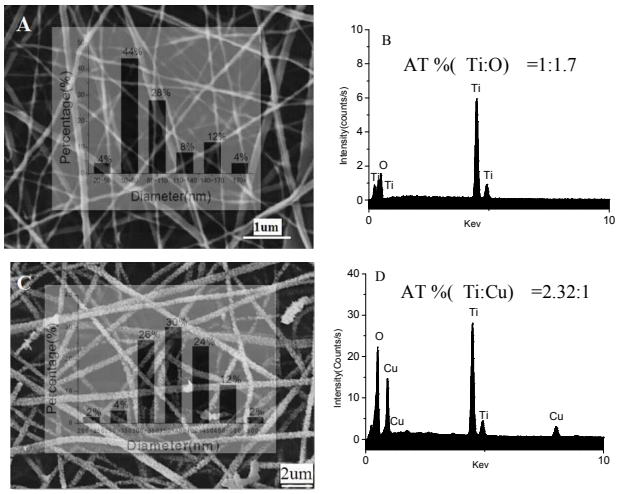

Fig.2 (A) The SEM images of TiO_2 nanofibers and statistics for diameter of the nanofibers TiO_2 fibers. (B) The EDS microanalysis on selected areas of TiO_2 nanofibers. (C) The

SEM of CuO/TiO_2 composite nanofibers heterostructure. (D) The EDS microanalysis on selected CuO/TiO_2 heterostructure.

The SEM image of low (Fig.3f) and high (Fig.3g) magnification show the high density of secondary CuO nanoparticles grown on the primary TiO_2 fiberous substrates. As we can see from Fig.3g that the CuO/TiO_2 fibers are full of pores on the surface, which may serve as transport paths for RhB molecules and utilize light sufficiently. So it is important for the properity of photocatalysis. The SEM image Fig.3a shows the morphology of CT2; the CuO shaped in spiny grew on the surface of TiO_2 nanofibers following the TEM picture (Fig.3c, Fig.3d).

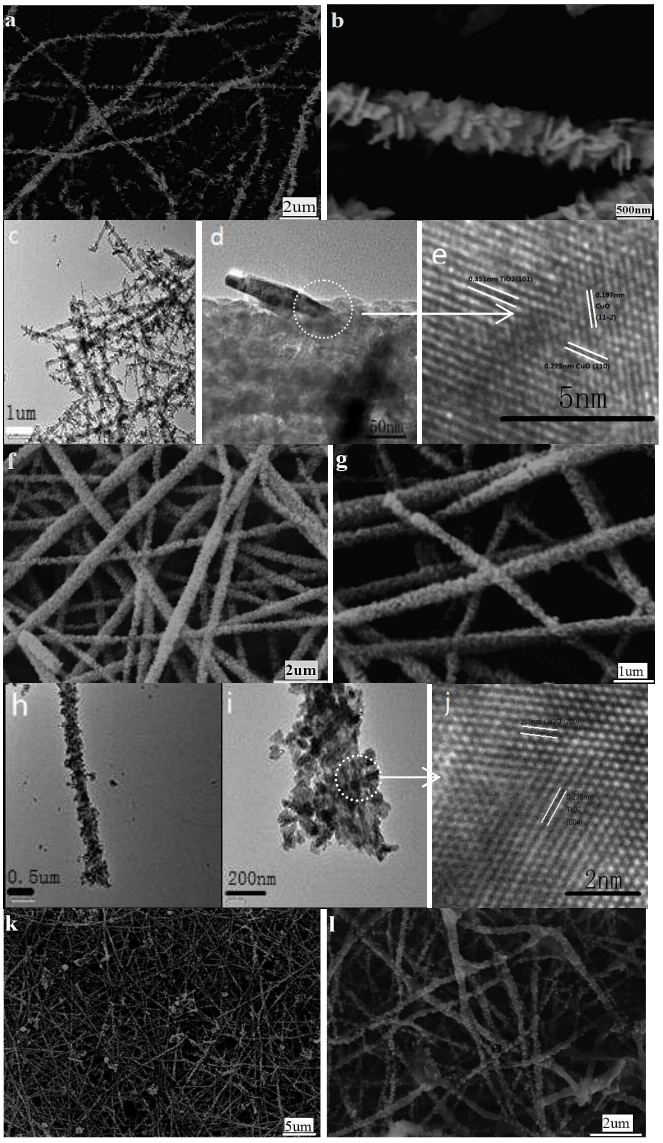

Fig.3 The SEM image (a) detailed view on CuO/TiO_2 hierarchical nanofibers of CT2 and a single nanofiber (b). (c) The TEM image of the CT2and (d) a single fiber. (e) The HRTEM image for the details of CT1. (f) The SEM image of the overall morphology of the CT1 sample. (g) The SEM image of the CT1 detailed view on CuO/TiO_2 nanofibers. (h) The TEM image of single fiber of CT1. (i) TEM of the detail CT1. (j) The HRTEM image of CT1. (k), (l) SEM images of CT1 (Five times after using).

Fig.3f and Fig.3g are the SEM images of CT1; the plenty of nanoparticles surround the TiO_2 fibers uniformly. The big difference in appearance between CT1 and CT2 is the different growth process in crystal growth. Ti-OH and Cu-OH would band together and leave a molecule of H_2O on the interfacial TiO_2 fibers. However, the CuO crystal in the process of growth would continue to grow in the same crystal form of CuO nanoparticles which grew on the TiO_2 fibers initially; thus formed the "section-section" structure of bamboo shoots (Fig.3b). The CT1 was used hexamine as the alkali source. Since the mixed solution was heated, hexamine would decompose into NH_3 and CH_2O and then the Cu^{2+} would be reduced into Cu^{+} by CH_2O. In other words, the size of CuO crystal would increase if the Cu^{+} was not formed. Because the two different lattices of CuO and Cu_2O would restrain the growth of the crystal, therefore the morphology of composite fibers are filled with nanoparticles of CuO and little Cu_2O. The XRD pattern could prove the results; the diffraction peaks in curve c (Fig.4) is the CT2 sample XRD pattern which shows the better crystallinity than that of CT1 in the curve b (Fig.4). The images of Fig.3k and Fig.3l were low and high magnification CuO/TiO_2 heterojunctions after five times resue and the morphology still keeped in good.

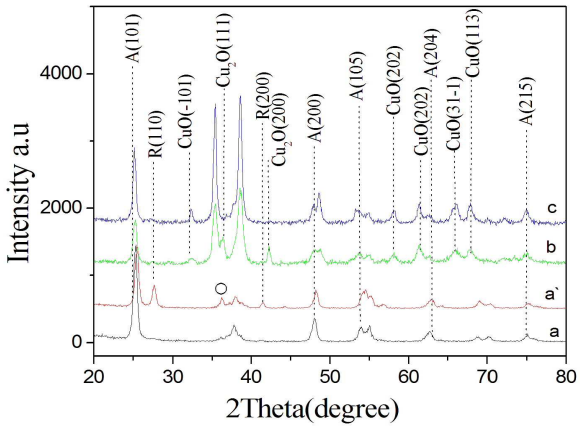

Fig.4 The XRD patterns of the as-synthesized products: (a) TiO_2 fibrous film. (a`) TiO_2 films after hydrothermal treatment. (b) CT1 hierarchical heterostructure. (c) The XRD curve of CT2

The phase and crystal structure of the sintering electrospun TiO_2 nanofibers and CuO/TiO_2 composite fibers were characterized by X-ray diffraction (XRD). Curve a (Fig.4a) showed the XRD pattern of pure TiO_2 nanofibers and the lattice parameters were a = 3.785 Å and c = 9.514 Å, which are close to the reported values[26] of the anatase phase. However, all the diffraction peaks of the TiO_2 sample can be indexed as well-crystallized tetragonal TiO_2 (JCPDS # 21-1272). It is important to note that the samples analyzed in the present work showed the presence of rutile (Fig.4a`) accompanying anatase after hydrothermal process, because the anatase would rearrange and form rutile under hydrothermal conditions.[27] There was a peak of rutile about 36° (marking) in the curve a`, but not in the curve b and c for the copper ions might blocking the transition of anatase.[28] Fig.4b is the XRD patterns of CT1, which indicates that the Cu_2O is mixed with the CuO/TiO_2 composite fibers. The 2θ = 42.30° is the typical diffraction peak of Cu_2O and the results could

be verified in the HRTEM of Fig.3j. The Fig.4c pattern which was the XRD pattern of CT2, which showed the crystallinity were better than CT1 for the sharp peaks.

The different morphology of the CuO on the fiber is mainly decided by alkali source. The hexamine would decompose into ammonia and formaldehyde gradually with the increase of temperature. Then the ammonia would combine the Cu^{2+} turning into Cu $(NH_3)_4^{2+}$. Small part of Cu $(NH_3)_4^{2+}$ would be reduced to Cu_2O for the existence of formaldehyde in the alkaline environment. Meanwhile, most Cu $(NH_3)_4^{2+}$ react with OH^- in aqueous solution and turn into CuO with the high temperature. As the large specific surface area of the TiO_2 nanofibers, it provides lots of active sites for the crystal growth of CuO. Moreover, as a result of the existence of the Ti-OH groups[30], it contributed to the formation of the bounds Ti-O-Cu, so the CuO would nucleate at the surface easily. According to the Oswald ripening mechanism[31], the seed crystal of CuO will get bigger following the increasing number of small crystal.

$$C_6H_{12}N_4 + H_2O \longrightarrow NH_3 + CH_2O$$

$$Cu^{2+} + 4NH_3 \longrightarrow Cu\ (NH_3)_4^{2+}\ (\text{mazarine})$$

$$Cu\ (NH_3)_4^{2+} + HCHO \longrightarrow Cu_2O + HCOONH_4$$

$$Cu\ (NH_3)_4^{2+} + OH^- \longrightarrow CuO + NH_3$$

$$Cu\text{-}OH + Ti\text{-}OH \longrightarrow Cu\text{-}O\text{-}Ti + H_2O$$

Photocatalytic oxidation of RhB

RhB is a chemically stable and poorly biodegradable dye for the difficulty to break chemical bonds and it is main contaminant in Water pollution of the environment. To prove the photocatalytic activity of CuO/TiO_2 films for the three-dimensional hierarchical heterostructure, we set up two sets of controlled trials using RhB as the degradation material. The blank test (Figure.5A) (without catalyst) under UV-vis light illuminations exhibited little photolysis about 10 % photodegradation efficiency for RhB in 3h. By contrast, when the CuO/TiO_2 films were used, the adsorption peak of the RhB at around 554 nm underwent fairly large decrease with irradiation for 3h about 95 %. We also investigated the photodegradation behaviors of RhB under continuous photocatalysis of the mixture of CuO and TiO_2 films (Single factor control variable method) according to the molar ratio in the EDS date of CT1 (Figure.2D). As we can see from the Figure.5B and Figure.5C, the CuO/TiO_2 composite fibers exhibited much higher photocalytic activity than the mixture of CuO and TiO_2 fiber. In addition, the catalyst we got had good reuse capacity; after five times reuse, the degradation ratio of RhB maintains 91.42 % and the ratio of recycled was still as high as 93 %. With the increase number of reuse, some CuO come off from the TiO_2 fibers (Fig.3k, Fig.3l) and a small amount of the loss when recycled were the main reasons for the slightly lower photocatalytic efficiency than before.

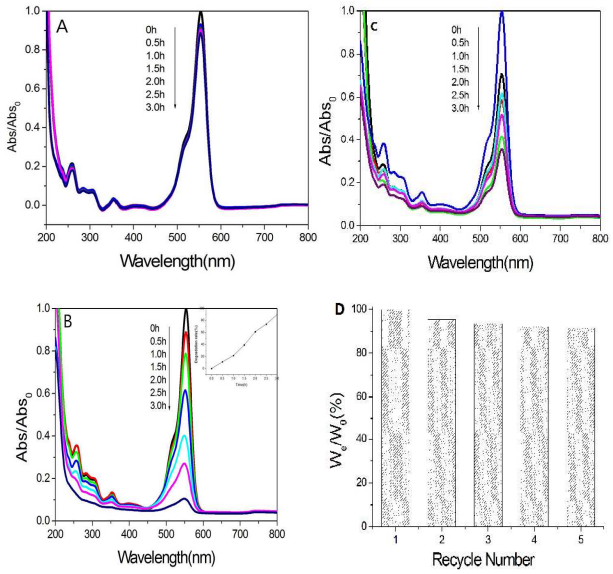

Fig.5 Curves of photocatalytic degradation of RhB under UV-light: (A) blank test. (B) In the presence of CuO/TiO_2 hierarchical heterostructure. (C) The test for the mixture of CuO and TiO_2 fibers. (D) The diagram of degradation ratio of RhB versus reuse times (The W_e indicates the degradation ratio of reuse times and W_0 indicates the first degradation ratio of RhB).

Comparing to the two results of Photocatalytic degradation experiments (Fig.5B, Fig.5C), the composite CuO/TiO_2 nanofibers showed higher Photocatalytic activity, therefore the CuO attaching on the surface of TiO_2 fibers played a great role in the the process of degradation of RhB. The band edge potentials of Cu^{2+}/Cu^0 and Cu^{2+}/Cu^+ (+ 0.34V and + 0.17V respectively)[32] are located below the conduction band edge of TiO_2 (− 0.2V),[33] When the heterojunction is irradiated by UV-light, the nano $Cu^{II}O$ could capture the electron from the surface of TiO_2 fibers. Since the Cu^{2+} ion has the unfilled 3d orbits ($3d^94s^0$ configuration), the reduction of Cu^{2+} is thermodynamically feasible (formula 1). The holes on the TiO_2 would be more and react with H_2O and produce radical species •OH followed by formula 2.

$$Cu^{II}O + e_{cb}^- \longrightarrow Cu^{I}O \qquad (1)$$

$$h_{vb}^+ + H_2O \longrightarrow \bullet OH + H^+ \qquad (2)$$

The electrons transfer to the nano-CuO and the charge will accumulate on the surface, therefore it must be consumed; some electrons would recombine with the photogenerated hole from the TiO_2 and react with oxygen to produce the •OH radicals after many transitions[34] (formula 3-6). The Cu^IO will be oxidized by the radical species which are generating from the reaction of electrons and oxygen.[35] Hence the Cu^IO would transform into $Cu^{II}O$ after the process of electron transfer. Ultimately, the recombination rate of electron hole pair should be reduced effectively. After a series of reactions, these reactive oxygen species ($\bullet O_2^-$ and •OH) diffusing in the solution would attack the chromophoric structure of RhB, leading to the cycloreversion of the RhB compounds according to the degradation curves (Fig.5B).[36]

$$e_t^- + O_2 \longrightarrow \bullet O_2^- \qquad (3)$$

$$e_t^- + O_2^- + H^+ \longrightarrow HO_2^- \quad (4)$$

$$HO_2^- + H^+ \longrightarrow H_2O_2 \quad (5)$$

$$H_2O_2 + e_t^- \longrightarrow \bullet OH + OH^- \quad (6)$$

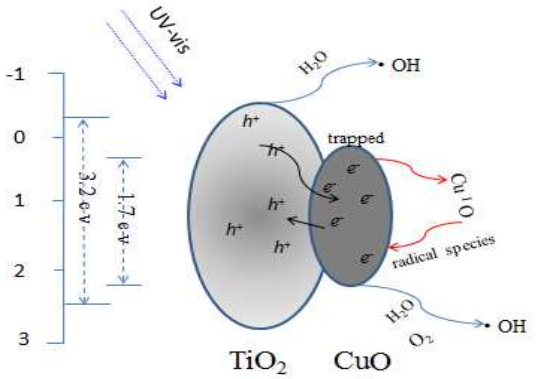

Fig.6 The mechanism of photocatalytic reactions on semiconductor photocatalyst

Conclusions

The 3D CuO/TiO_2 films were synthesized via a combination of an electrospinning method and a hydrothermal reaction. The morphologies of secondary nano-CuO appeared with different shapes by adjusting the experimental parameters. Moreover, the photocatalytic performance test and the results showed the composite CuO/TiO_2 fibers had better photocatalytic property than the mixture of CuO and TiO_2 films under same conditions. So the heterojunction of CuO/TiO_2 may possess great potential in the photocatalysts, sensors and other fields after further research.

Acknowledgements

This work was financially supported by the Basic research projects of JiLin province Science and Technology Agency (20130102040JC) and ChangChun Science and Technology plan projects (13NK01).

References

1 Fujishima, Akira, *Nature*, 1972, 238, 37-38.
2 Yangming Lin, Danzhen Li, Junhua Hu, Guangcan Xiao, Jinxiu Wang, Wenjuan Li and Xianzhi Fu, *J. Phys. Chem. C*, 2012, 116, 5764–5772.
3 Hui-Seon Kim, Jin-Wook Lee, Natalia Yantara, Pablo P. Boix, Sneha A. Kulkarni, Subodh Mhaisalkar, Michael Grätzel and Nam-Gyu Park, *Nano Lett*, 2013, 13, 2412–2417.
4 Che-Pu Hsu, Tsung-Wei Zeng, Ming-Chung Wu, Yu-Chieh Tu, Hsueh-Chung Liao and Wei-Fang Su, *RSC Adv*, 2014,4, 22926-22930.
5 Kyu-Shik Mun, Sara D. Alvarez, Won-Youl Choi and Michael J. Sailor, *ACS Nano*, 2010, 4, 2070–2076.
6 Yoshihisa Ohko Isao Ando, Chisa Niwa, Tetsu Tatsuma, Tsuyoshi Yamamura, Tetsuto Nakashima, Yoshinobu Kubota, and Akira Fujishima, *Environ. Sci. Technol*, 2001, 35, 2365-2368.
7 Shuhua Yao, Jinyang Li, Zhongliang Shi, *Particuology,* 2010, 8, 272-278.
8 Yanhui Ao, Jingjing Xu, Degang Fu, *Colloids and Surfaces A*, 2008, 312, 125–130.
9 Jian-hui Sun, Yong-kui Wang, Rui-xia Sun, *Materials Chemistry and Physics.*, 2009, 115, 303–308.
10 A.K. Ray Design, *Chemical Engineering Science*, 1999, 54, 3113–3125
11 Yupeng Zhang, Linfeng Fei, Xudong Jiang, Chunxu Pan, Yu Wang, *American Ceramic Society*, 2011, 94, 4157–4161.
12 SiMing Wang, XiaoJie Sun, *Advanced Materials Research*, 2013, 781-784, 1954-1957.
13 Markéta Zukalová, Jan Procházka, Arnošt Zukal, Jun Ho Yum, Ladislav Kavan, *INORG CHIM ACTA*, 2008, 361, 656-662.
14 Edward J. W. Crossland, Nakita Noel, VarunSivaram, Tomas Leijtens, Jack A. Alexander-Webber and Henry J. Snaith, *Nature*, 2013, 495, 215–219.
15 Yonghui Zhang, Suwen Liu, Zhiliang Xiu, Qifang Lu, Haiyan Sun, Guoshuai Liu , *Journal of Nanoparticle Research* , 2014, 2375, 1-9.
16 Munkhbayar. B, Dorjderem. M, Sarangerel. D, Ochirkhuyag, Bayanjargal, *Nanoscience and Nanotechnology Letters*, 2013, 5, 741-749.
17 In Gyoung Yu,Yong Joo Kim, Hark Jin Kim, Chongmu Lee and Wan In Lee, *J. Mater. Chem.*, 2011, 21, 532-538.
18 Y. K. Kim, E. Y. Kim, C. M. Whang, Y. H. Kim and W. I. Lee, *Sol-Gel Science and Technology.*, 2005, 33, 87-91.
19 Xiaodan Yan, Liang Feng, Jianguang Jia, Xiaowen Zhou and Yuan Lin, *J. Mater. Chem A.*, 2013, 1, 5347-5352.
20 Huanli Wang, Lisha Zhang, Zhigang Chen, Junqing Hu,Shijie Li, Zhaohui Wang, Jianshe Liu and Xinchen Wang, *Chem. Soc. Rev.*, 2014, 43, 5234-5244.
21 Kebin Zhou, Ruipu Wang, Boqing Xu and Yadong Li, *Nanotechnology*, 2006, 17, 3939-3943.
22 Xiaopeng Li, Ying Wang,Yu Leib and Zhiyong Gu, *RSC Adv*, 2012,2, 2302-2307.
23 M Frietsch, F Zudock, J Goschnick and M Bruns, *Sensors and Actuators B.*, 2000, 65, 379–381
24 O. Akhavan and E. Ghaderi, *Surface and Coatings Technology*, 2010, 205, 219–223.
25 Nuanxia Wang, Chenghua Sun, Yong Zhao, Shuyun Zhou, Ping Chena and Lei Jiang, *J. Mater. Chem*, 2008, 18, 3909–3911.
26 A. Kumar,R. Jose,K. Fujihara,J. Wang and S. Ramakrishna, *Chem. Mater*2007, 19, 6536–6542.
27 Kazumichi, Yanagisawa, James Ovenstone. *J. Phys. Chem. B.,* 1999, 103, 7781-7787
28 K. Wilke, H.D. Breuer, *Journal of Photochemistry and Photobiology A: Chemistry*, 1999, 121, 49-53
29 Cao, X. B.; Lan, X. M.; Guo, Y.; Zhao, C.; Han, S. M.; Wang, J.; Zhao, Q. R. *J. Phys. Chem. C,* 2007, 111, 18958–18964.
30 Y. Masuda, S. Ieda, K. Koumoto. *Langmuir*, 2003, 19, 4415–4419.
31 Huogen Yu, Jiaguo Yu, Shengwei Liu and Stephen Mann, *Chem. Mater.*, 2007, 19, 4327 – 4334.
32 K.chiang, R.Amal*, T. tran. *Advances in Environmental Research* 2002, 6, 471 - 485.
33 Fox. M.A., Dulay, M.T. Chem. Rev, 1993, 93, 341 – 304.

34 Heinz Gerischer and Adam Heller, *Journal of Physical Chemistry*, 1991, 95, 5261-5267.
35 Viviana Maria da Silva Rocha, Madson de Godoi Pereira, Leonardo Ribeiro Teles, Marluce Oliveira da Guarda Souza*. *Materials Science and Engineering B*, 2014, 185, 13-20.
36 Jiandong Zhuang, Wenxin Dai, Qinfen Tian, Zhaohui Li, Liyan Xie, Jixin Wang and Ping Liu, *Langmuir*., 2010, 26, 9686 – 9694.

